Investigation Of Gas Bubble Velocities From Experimental Data Of Ultrafast Two-Layer Electron Beam X-Ray Tomography

Anindityo Patmonoaji[1*], Manuel Banowski[2], Dirk Lucas[2], Deendarlianto[1]

[1]Graduate Department of Mechanical Engineering GadjahMada University
Jl. Grafika No. 2, Yogyakarta, 55281, Indonesia
[2]Helmholtz-Zentrum Dresden-Rossendorf
BautznerLandstr, 400, D-01328 Dresden, Germany

Abstract: At the Institute of Fluid Dynamics in Helmholtz-Zentrum Dresden-Rossendorf (HZDR) a unique ultrafast X-ray tomography named ROFEX (Rossendorffast electron beam X-ray tomography) was developed. This non-intrusive measurement technique with high spatial and temporal resolution enables to measure gas liquid phase distribution with frame rate up to 8000 Hz for simultaneous dual layer measurement and a spatial resolution of 2 mm. Presently gas bubble velocities are determined by performing cross-correlation from dual measurement layers data which results in radial averaged gas velocity profiles. In this work a new improved method has been developed which has capability to derive velocities of single gas bubble inside the flow. The new method works by pairing the correct bubbles that are detected at both measurement layers. In order to acquire the correct bubble pairs, comparison of bubble parameters such as volume, detected position and resulting bubble velocity are used. When the correct bubble pair has been found, the difference of bubble time shift between both measurement layers can be determined. Therefore, gas bubble velocity is obtained by dividing the measurement layer distance with difference of bubble time detection. In this paper, detailed explanation of the algorithm working principle is given. The algorithm was validated using phantom data and was tested for some flow characteristic. Radial average velocity profils obtained by this method were also compared with the results from the cross-correlation method. The bubble velocity is also computed for investigation of gas bubbles movement behavior and physical mechanism.

1. Introduction

Gas – liquid flows in vertical pipesare commonly found in many industrial applications such asat petroleum industry, power plants, and any other chemical process equipment. Investigations of gas – liquid flows have been carried out to determine the physical phenomena inside the flow. Through deeper understanding of gas – liquid flow behavior inside a pipe, an improvement of gas – liquid flow application can be achieved.

In the following centuries, studies of gas – liquid flow pattern were performed with a lot of measurement system types and various concepts. For most diluted flow, various measurement system especially optical method are able to capture the phenomena in quite satisfying result. However for dense flow, available measurement systems are still insufficient to acquire necessary data from the phenomena.

On the basis of developing new advance two-phase flow Computation Fluid Dynamics (CFD) models to reduce expensive experiments to prove the safety especially in nuclear safety research,an advance measurement system which has capability to capture the important phenomena of gas – liquid phase flow in detail and accurate is really needed. It is surely needed for understanding the physical mechanism of flow phenomena and also especially for improvement and validation of new two phase flow simulation code model.

At the Institute of Fluid Dynamics at Helmholtz-Zentrum Dresden-Rossendorf a unique ultrafast X-ray tomography named ROFEXis developed. ROFEX is capable to reach a frame rate up to 8 kHz for simultaneous dual layer measurement and also spatial resolution down to 2 mm. For various gas-liquid flow measurement, ROFEX shows promising result to measure detail and accurate of gas-liquid phenomena.

ISBN 978 979 8510 61 8

2. Experimental Setup

The experiment is conducted in Transient Two – Phase Flow test facility(TOPFLOW) at the Institute of Fluid Dynamics in HZDR. TOPFLOW allows air-water experiment at temperature of 30°C and pressure about 4 bars. Steam-water experiments with a pressure up to 7 MPa and saturation temperature at 286°Care also able to be conducted in this test facility. Maximum 50 kg/s saturated water mass flow rate through the vertical test section and 1.4 kg/s of maximum steam mass flow rate are available to be produced by a 4MW electrical heater. This test facility is described by Prasser et al. (2006).

Inside the TOPFLOW facility, the test section for ROFEX measurements is installed, shown in Figure 1. A titanium pipe with inner diameter (ID) of 54.8 mm with total length of 6 m was installed. The purpose of the application of titanium as the pipe material is to reduce wall thickness for

steam-water flow experiment up to 1.6 mm in order to maintain operation pressure of 7 MPa. This reduction of pipe wall thickness reduces the radiation attenuation which provides better signal to noise ratio for radiation measurement. The ROFEX scanner is mounted on a vertical

elevation unit which allows lifting of the height of the

scanner into different measurement position from L/D = 0 up to L/D = 60.

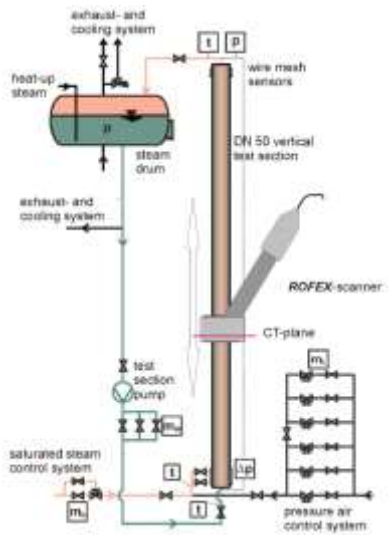

Figure 1. Test Section

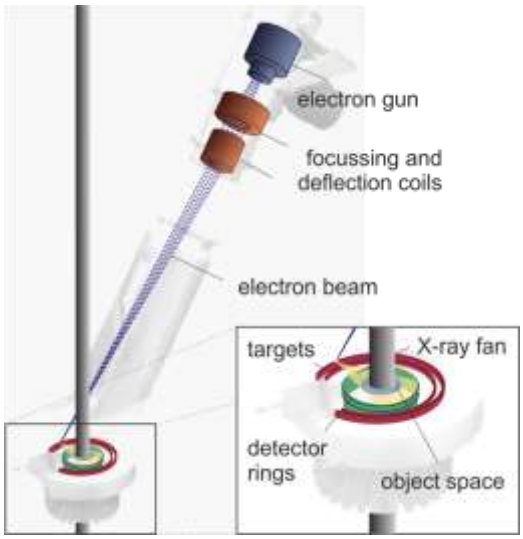

Figure 2. ROFEX scanning system

ROFEX is a unique ultrafast electron beam X-ray tomography that works according to the scanned electron beam principle to perform scanning around the object instead of mechanical rotating part, presented by Hampel et al. (2005). Electron beam is used to achieve high frame rate up to thousand kHz which is the required frame rate to capture air-gas flow phenomena inside a pipe. The schematic design of ROFEX is shown in Figure 2.

In every measurement, two measurement layers with axial distance of 10.2 mm are employed for investigation of gas bubble axial velocity. Each of measurement is conducted for 10 seconds with frame rate between 1000 Hz – 2500 Hz depend on the flow velocity. Detail explanation about ROFEX is described by Fischer et al. (2008) and Fischer and Hampel (2010).

3. Data Processing

3.1 Image Reconstruction

During image reconstruction, attenuation X-ray distribution captured by the detector ring is processed with filtered back projection algorithm from Kak and Slanley (1988). After the utilizing the filtered back projection algorithm, 3D array with gray value that represent the distribution image of the liquid and gas phases is obtained. This 3D array represents the reconstructed data in spatial resolution by square pixel of 0.5 mm and temporal resolution by frame rate in axial direction. The 3D image and the cross sectional cut of the reconstructed image is shown Figure 3.

ISBN 978 979 8510 61 8

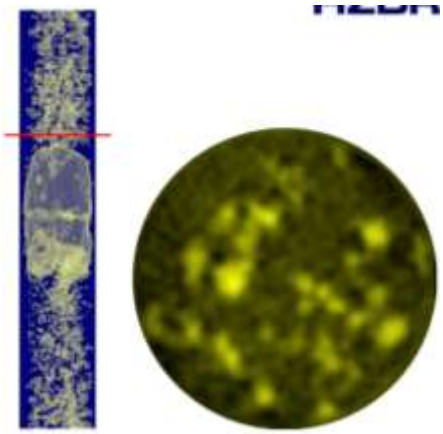

Figure 3. Reconstructed image of3D array (left) and cross-section (right) of the flow

3.2 Bubbles Segmentation

In order to calculate bubble parameters, a binarization between gas and liquid flow is needed, shown in Figure 4. Banowski et al. (2013) developed a successful improvement algorithm for ROFEX bubble segmentation. The segmentation algorithm works by finding the local maximum gray values and perform agglomeration with the surrounding connected pixels. If no more agglomeration is possible, growing of bubble regions which are larger than the real bubble is performed. To obtain real bubble size, individual bubble threshold depending on maximum bubble gray value is used. This process is starting from maximum gray value of 95% until 10% and performs repeatedly with decreasing 10% of the maximum gray value in every step.

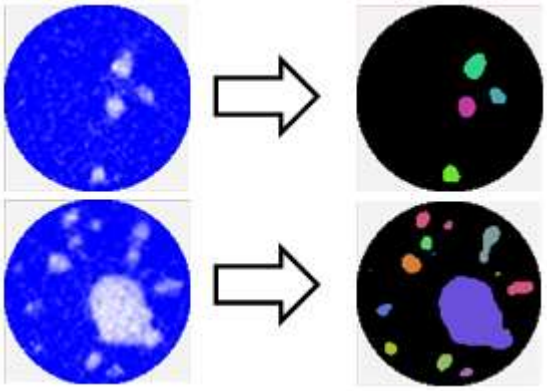

Figure 4. Bubble segmentation visualization

After binarization is performed, bubble parameters such as bubble virtual size, bubble position, and bubble detected time are able to be derived, that is using the method used byPrasser et al. (2001), Prasser et al. (2002). . A bubble virtual size term is used because the unit is in mm^2ms.

3.3 Bubble pairs Selection

In order to derive bubble actual size, bubble velocity is needed. Therefore bubble velocity is calculated by pairing each bubble that is detected at lower measurement layer to upper measurement layer. Bubble pairing start from largest bubble size to smallest bubble size. When the bubble pairing has found the most probable pair, both bubbles are labelled as solved bubble to prevent bubble with multiple pairs.

Even though the idea sounds simple, a difficulty appears when numerous gas bubbles are detected. Therefore certain gas bubble parameters such as bubble virtual size, position, detected time, and even specific flow condition insidethe flow are used as crucial information to identify the correct bubble pairs. Therefore specific probability functions for the compared parameters are created. Bubble with the closest value with the bubble at the other plane and the expected value is having high probability.

a. Volume Probability

Bubble pairs with the most similar volume have the highest volume probability as the correct bubble pairs. In order to calculate the volume probability, Gaussian function is used (equation 1).

$$\emptyset_{\mathrm{vol}} = e^{0.5\left(\frac{\Delta_{\mathrm{vol}}{}^2}{\sigma_{\mathrm{vol}}{}^2}\right)} \qquad (1) \quad \text{with } \sigma_{\mathrm{vol}} = 10^{-2}\mathrm{n}^2 + 0.3309\mathrm{n} + 10.586$$

The delta volume (Δ_{vol})represents the difference of bubble virtual volume from both measurement layers. Sigma volume(σ_{vol})is a parameter of the Gaussian function that is used as a function describing the tolerance of volume. This function represents the superposition of a ± 0.5 mm^2ms diameter tolerance for small bubbles (discritization error) and 10% of diameter tolerance for larger bubbles (general uncertainty range).

b. Position Probability

Despite of flow disturbance effect around bubbles, they move only for low distance at horizontal direction. Therefore bubble pairs with the similar detected position arehaving highest position probability. Gaussian function is also used to calculate the position probability (equation 2).

$$\emptyset_{\mathrm{pos}} = e^{0.5\left(\frac{\Delta\mathrm{pos}^2}{\sigma\mathrm{pos}^2}\right)} \qquad (2) \quad \text{with } \sigma_{\mathrm{pos}} = \frac{\tilde{\mathrm{A}}}{\mathrm{U}_{\mathrm{axial}}}$$

The delta position represents the difference of bubble detected position from both measurement layers.Sigma position is used as a function that describes the tolerance of bubble crosssectional movement. This function represents that if a bubble rises in high velocity, the probability to move at crosssectional direction is only smaller than bubble that rises in low velocity. The rate of cross-sectional area probability movement increase is represented by variable $\tilde{A}$ with a unit of mm^2/ms.The value of $\tilde{A}$ iis between 2.5 to 5 mm^2/ms and depends on flow disturbance condition.

c. Velocity Probability

The velocity probability is a crucial parameter obtaining correct bubble pairs. This probability determines in which time coordinate range the correct bubble pair should be

located. Because the bubble rising velocity is also affected by the flow condition around it, specific conditions for these probabilities are needed.

For the determination of the expected velocity, the power law distribution from Bankoff (1960) is used for the radial velocity profile (equation 3.1) and equation from Harmathy (1960) is used for calculating the bubble rise velocity (equation 3.2). Hence the expected velocity is the velocity of the surrounding bubble location adds with the bubble drift velocity (equation 3). For defining a velocity tolerance range, a value of 0.375 of the expected velocity is taken for the tolerance which is chosen to give enough tolerance for bubble that has a different velocity behavior.

$$U_{exp} = U_{pro} + U_{drift} \qquad (3)$$

$$U_{pro} = 1.2U_M\left(1 - \frac{r}{R}\right)^{1/n} \qquad (3.1) \quad \text{with } U_M = U_{SG} + U_{SL}$$

$$U_{drift} = 1.53\left(\frac{g\,\Delta\rho\,\gamma}{\rho_L}\right)^{1/4} \qquad (3.2)$$

In calculation of velocity probability, three conditions are created. First condition is when the bubble pairs velocity is still in the first range of velocity tolerance range. In this bubble pairss have a velocity probability between 0.8 and 1 that decrease linearly from the point of expected velocity to the point of

first range of velocity tolerance. Second condition follows when the bubble pairs velocity is in the second range of velocity tolerance range. In this range bubble pairs has a velocity probability between 0 until 0.8. The velocity probability decreases linearly from 0.8 at the first range of deviation of velocity to 0 at the second range of deviation of velocity. The third condition occurs when the bubble pairs velocity is in the range of third until unlimited range of velocity tolerance range. This condition result in zero velocity probability for all bubble pairss inside this condition. These conditions are represented by Figure 5 and equation below(equation 4).

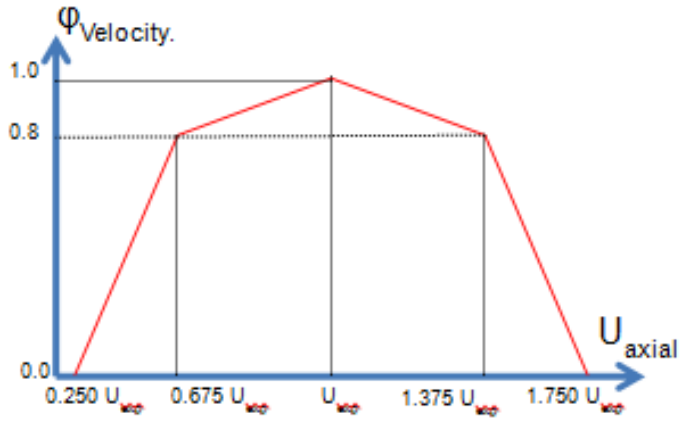

Figure 5. Velocity Probability Chart

$$\phi_{vel}\begin{cases} 0.8 + 0.2\left(\dfrac{U_{bp} - \left(\mathrm{U_{exp}} - U_{range}\right)}{U_{range}}\right) \longrightarrow & 0.625\ \mathrm{U_{exp}} < \mathrm{U_{bp}} < \mathrm{U_{exp}} \\ 1.0 - 0.2\left(\dfrac{U_{bp} - \mathrm{U_{exp}}}{U_{range}}\right) \longrightarrow & \mathrm{U_{exp}} < \mathrm{U_{bp}} < 1.375\ \mathrm{U_{exp}} \\ 0.8\left(\dfrac{U_{bp} - \left(\mathrm{U_{exp}} - 2U_{range}\right)}{U_{range}}\right) \longrightarrow & 0.250\ \mathrm{U_{exp}} < \mathrm{U_{bp}} < 0.625\ \mathrm{U_{exp}} \\ 1.0 - 0.8\left(\dfrac{U_{bp} - \left(\mathrm{U_{exp}} + U_{range}\right)}{U_{range}}\right) \longrightarrow & 1.375\ \mathrm{U_{exp}} < \mathrm{U_{bp}} < 1.750\ \mathrm{U_{exp}} \\ 0 \longrightarrow & 0.250\ \mathrm{U_{exp}} > \mathrm{U_{bp}} \text{ and } \mathrm{U_{bp}} > 1.750\ \mathrm{U_{exp}} \end{cases} \quad (4)$$

d. Special case "slug flow"

In a presence of Taylor bubble, the flow condition around thisTaylor bubble is highly affected by this. Therefore expected velocity of affected regions around Taylor bubble is also specified, shown in Figure 6. In this calculation, Taylor bubble is described as bubble with a diameter larger than 20 mm and gas void fraction at its center larger than 0.45 in cross section. The expected velocity of the Taylor bubble is calculated with equation 5 taken from Nicklin (1962).

Taylor Bubble

$$U_{exp} = U_{TB} = 1.2U_c + 0.35\sqrt{gD} \quad (5)$$

Falling Film Region

$$U_{exp} = U_M + U_{drift} + U_f \quad (6.1)$$

$$U_f = -(U_{TB} - U_M)\frac{A_{TB}}{A_f} \quad (6.2)$$

Wake Region

$$\sigma_{vol} = 2(10^{-2}n^2 + 0.3309n + 10.586) \quad (7)$$

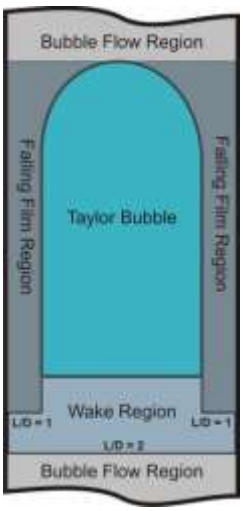

Figure 6. Regions partition around Taylor bubble

The falling film region is described as region located between Taylor bubble and pipe wall and detected between Taylor bubble nose up to 1 pipe diameter after Taylor bubble tail (cf. Figure 6). The specification of one pipe diameter after Taylor bubble tail follows the description of falling film penetration by Kawaji et al. (1997). The expected falling film velocity is calculated using mass continuity between rising Taylor bubble and falling film adds with the bubble rise velocity (equations6.1 and 6.2).

The wake region is created to overcome toroidal vortices produced by the Taylor bubble. This region is assigned as zone until 2 pipe diameters after Taylor bubble tail(van Hout et al., 2002) excluding the falling film region. Caused by a high coalescence rate in the wake, solving a bubble in two bubble pairs is allowed and the sigma volume is two times higher than in bubble flow conditions (equation 8).

e. Total Probability

After all of the parameter probabilities have been calculated, the total probability of the selected bubble is calculated by multiplying all of the probability parameters (equation 8).

$$\emptyset_{\text{total}} = \emptyset_{\text{vol}}\emptyset_{\text{pos}}\emptyset_{\text{vel}} \quad (8)$$

The Bubble pairwith the highest total probability is selected as the correct bubble pair and labelled as solved bubble. However, bubble with maximum total probability less than 0.25 is assumed to have no pair to prevent wrong bubble selection.

3.4. Bubble pairs Velocity Calculation

Once the bubble pairss have been obtained, the different of bubble time detection can be derived to calculate the resulting velocities. Since the bubbles inside the flow may resemble a large range of bubble sizes, a reference point to calculate the bubble time detection is also adapted dependent on the bubble size. For small size bubble (D_e < 5 mm), the bubble center is used. Therefore for large size bubbles (D_e > 20 mm), the bubble nose is used to prevent instability of changing shape or bubble coalescence. However bubbles with a diameter between 5 mm and 20 mm use a linearly interpolated point between center and nose (equation 9).

$$I_{vir} = I_{cm} + (I_{cm} - I_{nose})\frac{(D_e - 5)}{15} \quad (9)$$

4. Results and Discussion

4.1 Phantom measurements

In order to validate the measurements, a phantom is used. The phantom is madeby300 milled plastic slides stacked up vertically. During scanning, these milled holes are similar to gas bubbles. In order to

simulatean artificial bubble rising velocity, the phantom is pulled vertically using a crane with known velocity.

During phantom data processing, the expected velocity for the calculation is adapted to be equal with the crane pulling velocity that is 0.556 m/s. Processing of this phantom data result in 96.88% of solved bubble with 5% from wrong bubble pairs selection which can be observed at the scattering in Figure 7. However agood agreement of solved bubble velocity distribution with the pulling velocity is obtained.

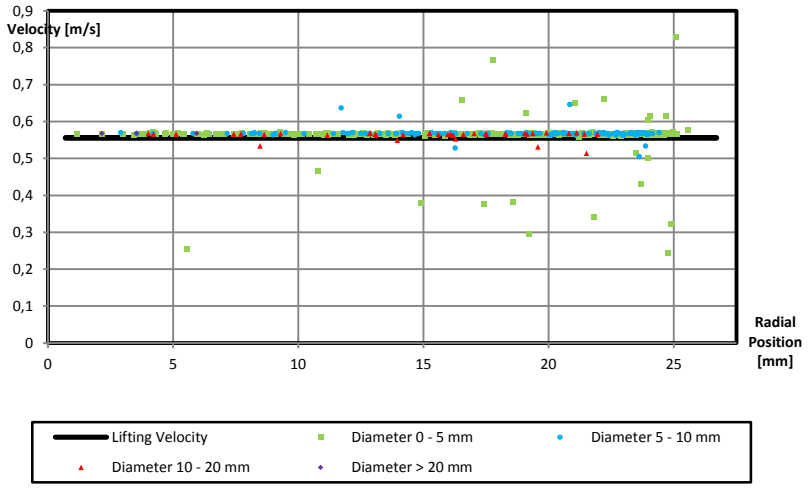

Figure 7. Solved bubbles distribution for phantom data set

4.2 Real two-phase flow measurements

For real air-water flow measurement, bubble flow and slug flow were processed. The specified flow ratesare shown in Table 1 for two exemplary chosen two-phase flow regimes.

Table 1. Air-water flow measurement specification

Flow Pattern	J_L[m/s]	J_G[m/s]	L/D
Bubble Flow	0.405	0.0151	60
Slug Flow	1.017	0.219	60

For the bubble flow, a solved bubble rateof 97.26 % is reached. The side cut views of both measurement planes are

shown in Figure 8. Bubbles with the same colour are assigned as bubble pairs. Figure 9 shows the comparison of the radial velocity profiles by the averaged solved bubble pair velocities and the cross-correlation result described in Prasser et al. (2005). A more detailed distribution of the solved bubble pair velocitiesagainst their radial position is plotted in Figure10. The scattered pointsbelow the cloud in the pipe center arecaused by wrong bubble pair assignment. Reasons for the wrong pair finding are mainly because of coalescence effects. However their rate to the correct found bubble pairs is very low. Figure 11 shows the bubble flow velocities as vector field view. It can be observed that bubbles located at pipe center move faster than bubbles located at pipe wall due to the dependency on surrounding liquid velocity

.

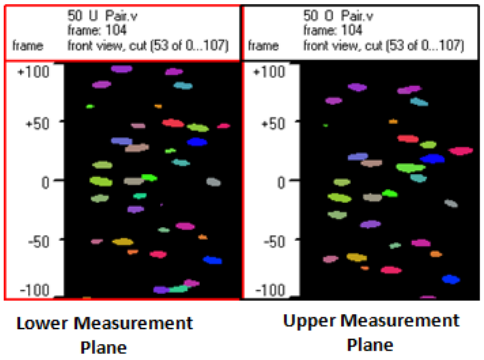

Figure 8. Image of bubble selection from front cut view for bubble flow

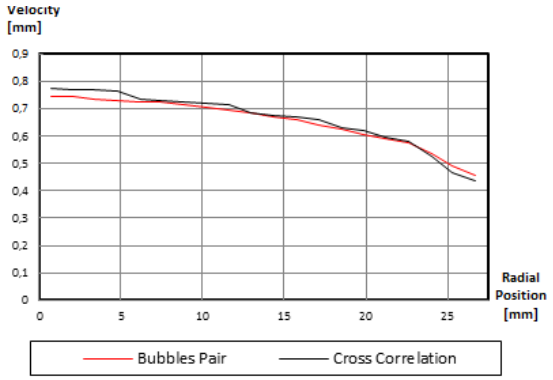

Figure 9. Comparison of radial average velocity from bubble pairs and cross-correlation for bubble flow

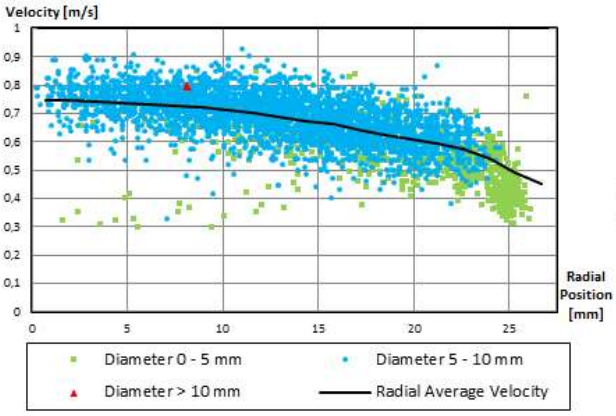

Figure 10. Solved bubbles distribution for bubble flow

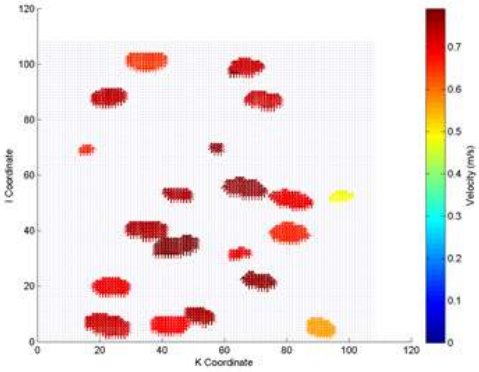

Figure 11. Bubble flow velocity field

For the slug flow, a solved bubble rateof 73.67 % is reached. However the most of large size bubble are solved, so the rate of void fraction of the solved bubbles to the total void fraction amounts 91.56 %. The side cut views of both measurement planes areshown in Figure 12. In Figure 13, the comparison ofthe radial velocity profiles by the averaged solved bubble pair velocities and the cross-correlation result shows a little disagreement in the radius range r = 10…24 mm.The higher velocities of the averaged bubble pair profile is a reason by averaging depending on volume fractions. So, the large Taylor bubbles have a higher influence to the velocity profile and overestimate the profile. The cross-correlation method needs many gas bubbles for a stable correlation function, so the velocities of smaller bubbles determine mainly the velocity profile and underestimate the profile. The single bubble velocities against their pipe radial position are plotted in Figure 14. It can be observed that the scattering is caused mainly by the small bubbles. At the image of velocity field (Figure 15), the effect of Taylor bubble and theirnose surrounding is observable. The Taylor bubble tends to push away other bubbles and drain them into the region of falling film.

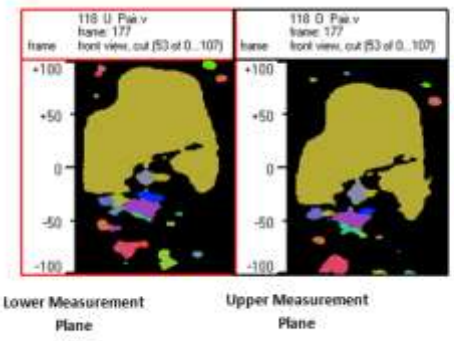

Figure 12. Image of bubble selection from front cut view for slug flow

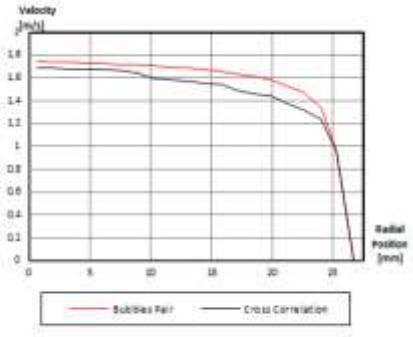

Figure 13. Comparison of radial average velocity from bubble pairs and cross-correlation for slug flow

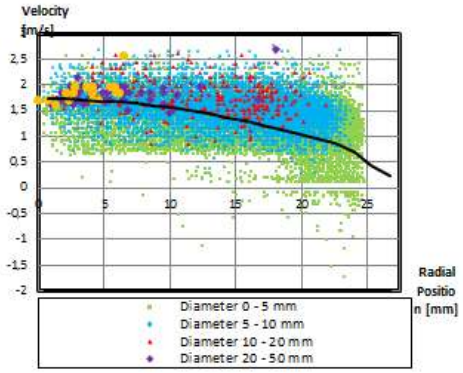

Figure 14. Solved bubbles distribution for slug flow

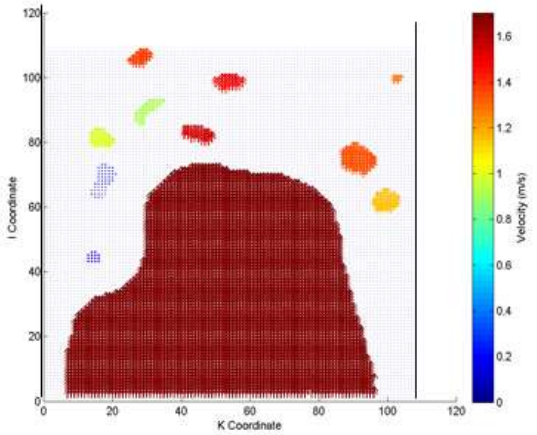

Figure 15. Slug flow velocity field

5. Uncertainties and Limitations

The uncertainties of the measurement is calculated by comparing the set value of the gas superficial velocity injected to the pipe with the computed gas superficial velocity from the ROFEX measurements, shown in Table 2. In order to calculate the measured gas superficial velocity, the bubble volume fraction is multiplied with the bubble velocity. However for the unsolved bubbles, the bubble volume fraction is multiplied with the radial average velocity depending on their radial position.

It can be observed that the error of gas superficial velocity detection is mostly below 10 % which shows a good agreement for the measurement. The percentage of the solved bubble is also quite high, mostly greater than 90 % for bubble flows and mostly greater than 75 % for slug flows. For the percentage of the solved gas fraction, it can be seen also that the value is higher than 90 % except for the first slug flow case. The reason for this case is caused by the flow condition. It is a quite bubble dense especially in wake regions after Taylor bubbles. Therefore the bubble segmentation found difficulties to separate each bubble.

In the current progress, this bubble velocity calculation method is still inapplicable for annular flow. During annular flow, the flow is mainly contained gas at the center of pipe which looks like a Taylor bubble with unlimited length. Therefore the bubble center or bubble nose coordinate cannot be obtained correctly. Though there are some liquid lamellae inside the gas phase, the bubble segmentation is still unable to separate the gas phase correctly.

Flow Pattern	J_L [m/s]	$J_{G\ Set}$ [m/s]	$J_{G\ Meas}$[m/s]	$\frac{(J_{G\ Meas} - J_{G\ Set})}{J_{G\ Set}}$	Percentage of Solved Bubble	Percentage of Solved Gas Fraction
Bubble Flow	0.0405	0.0096	0.0100	4%	89.50%	93.58%
	0.161	0.0096	0.0096	0%	97.33%	97.73%
	1.017	0.0096	0.0104	8.33%	97.05%	98.48%
Slug Flow	0.161	0.219	0.2166	-3.79%	80.27%	73.64%
	0.405	0.219	0.2256	3%	82.08%	93.69%
	1.017	0.219	0.2570	15.86%	73.67%	91.56%

Table 2.Comparison of set value of gas superficial velocity with the measured

6. Conclusion

A new method for computing bubble velocitiesin gas-liquid flows has been developed. Through finding of bubble pairs, single gas bubble velocities can be derived in a good agreement result with phantom measurements.The solved bubble rate amounts 96.88 % with 5 % of wrong bubble pairs selection errors is reached.

For air-water flows, the bubble pair method also results in a good agreement with the cross-correlation method which is the common used method to calculate gas velocitiesof ROFEX measurement data. However the bubble pair method shows more benefits; single gas bubble velocity of bubbles inside gas-liquid flow is able to be derived. Therefore the movement and velocity of each bubble can be observed and studied.For the shown examples, an averaged solved bubble ratearound 90 % is reached

for bubble flows and 75 % for slug flows. However for the void fraction of the solved bubbles is more than 90 % for almost of both flow regimes.
The uncertainties of the measurement are almost less than 10 % for both flows, which are quite satisfying results. The uncertainties are calculated by computing the superficial gas velocity using the measurement results. However for annular flow measurements, this presented method is still unable to calculate the gas phase velocity since reference point for bubble time detection unable to be located correctly.

7. Nomenclatures

A	Area (m^2)
Ã	Rate of possibility area increase (mm^2/ms)
D	Pipe diameter (m)
G	Gravitational constant (9.81 m/s^2)
n	Bubble Voxel Number
U	Velocity (m/s)

Greek letters

Δ	Deviation parameter
γ	Surface tension (N/m)
Σ	Tolerance parameter
∅	Probability
Σ	Density (kg/m^3)

Subsripts

Bp	Bubble pairs
C	Center pipe line
Drift	Drift
Exp	Expected
F	Film
M	Mixture
Pos	Position
Pro	Radial velocity profile
range	Range
Tb	Taylor bubble
Vol	Volume
vel	Velocity
total	Total

8. References

1. Bankoff, S. G. (1960). A variable density single-fluid model for two-phase flow with particular reference to steam-water flow. J. Heat Transfer, vol. 82 (2), pp. 265-270.
2. Banowski, M., Lucas, D., Hoppe, D., Beyer, M., Szalinski, L., Hampel, U. (2013).Segmentation of ultrafast x-ray tomographed gas-liquid flows in a vertical pipe at differenct flow regimes, WCIPT7 2013, Krakow.
3. Fischer, F., Hoppe, D., Schleicher, E., Mattausch, G., Flaske, H., Bartel, R., Hampel, U. (2008). An ultra fast electron beam x-ray tomography scanner, Measurement Science and Technology, Vol. 19.
4. Fischer, F. and Hampel, U. (2010). Ultra-fast electron beam X-ray computerd tomography for two-phase flow measurement, Nuclear Engineering and Design, vol. 240, pp. 2254-2259.
5. Hampel, U., Speck, M., Koch, D., Menz, H.-J., Mayer, H.-G., Fietz, J., Hoppe, D., Schleicher, E., Zippe, C., Prasser, H.-M. (2005), Experimental ultra fast X-ray computed tomography with a linearly scanned electron beam source, Flow Measurement and Instrumentation, Vol. 16, 65-72.
6. Harmathy, T. Z. (1960). Velocity of large drops and bubbles in media infinite or restricted extent, AIChE J., 6, 281.
7. Kak, A. C. and Slaney, M. (1988). Principles of computerized tomographic imaging, IEEE Press.
8. Kawaji, M., DeJesus, J.M., Tudose, G. (1997). Investigation of flow structures in vertical slug flow,

Nuclear Engineering and Design, vol. 175, pp. 37-48.
9. Nicklin. D.J., Wilkes, J.O. and Davidson, I.F.(1962).

Two Phase Flow in VerticalTubes,Trans. Inst. Chem.-Engrs., 40,61.
10. Prasser, H. M., Scholz, D., & Zippe, C. (2001). Bubble size measurement using wire-mesh sensors. *Flow measurement and Instrumentation*, *12*(4), 299-312.
11. Prasser, H. M., Krepper, E., & Lucas, D. (2002). Evolution of the two-phase flow in a ve rtical tube—decomposition of gas fraction profiles according to bubble size classes using w ire-mesh sensors. *International Journal of Thermal Sciences*, *41*(1), 17-28.
12. Prasser, H.-M., Beyer, M., Carl, H., Manera, A., Pietruske, H., Schütz, P., Weiβ, F.-P. (2006). The multipurpose thermal-hydraulic test facility TOPFLOW : an overview on experimental capabilities, instrumentation and results, *Kerntechnik*, vol. 71, pp. 163-173.
13. Prasser, H.-M., Beyer, M., Böttger, A., Carl, H., Lucas, D., Schaffrath, A., Schütz, P., Weiss, F.-P., Zschau, J. (2004). Influence of the pipe diameter on the liquid interface in a vertical two-phase pipe dlow.
14. vanHout, R., Gulitski, A., Barnea, A., Shemer., L. (2002). Experimental investigation of the velocity field induced by a taylor bubble rising in stagnant water, Int. J. Multiphase Flow, vol. 28, pp. 579-596.

Acknowledgement

This work is carried out in the frame of a current research project funded by the German Federal Ministry of Economics and Technology, project number 150 1411.